A Scalable Model for Human Scala-Tympani Phantoms

James R. Clark[1]
Department of Mechanical Engineering,
University of Utah,
Salt Lake City, UT 84112
e-mail: james.r.clark@utah.edu

Frank M. Warren
Department of Otolaryngology,
Division of Otology and Skull Base Surgery,
Oregon Health and Science University,
Portland, OR 97239
e-mail: warrenf@ohsu.edu

Jake J. Abbott
Department of Mechanical Engineering,
University of Utah,
Salt Lake City, UT 84112
e-mail: jake.abbott@utah.edu

In cochlear-implant (CI) insertion experiments, scala-tympani (ST) phantoms are often used in place of in vivo studies or cadaver studies. During the development of novel CI technology, a scaled-up phantom is often desirable. In this paper, we create a scalable model of the human ST by synthesizing published anatomical data and images. We utilize the model to fabricate an accurate, inexpensive, and reproducible ST phantom at a 3:1 scale. [DOI: 10.1115/1.4002932]

Keywords: scala tympani, cochlea, phantom, model, cochlear implant, parametric

1 Introduction

Cochlear implants (CIs) can restore some functional hearing for individuals with profound sensorineural hearing loss. A cochlear implant directly stimulates the user's auditory nerve using electrical impulses delivered via an electrode array. The array consists of electrodes spaced along a silicone carrier, which is optimally inserted into the scala-tympani (ST) chamber of the cochlea, a spiral-shaped organ in the inner ear. Insertion of the CI has been shown to result in damage to delicate intracochlear structures, and correct placement of the electrode array can be difficult to achieve. Because of this, recent CI research efforts have focused on decreasing insertion trauma and achieving better array placement within the ST. Insertion experiments are frequently performed as part of this research to evaluate electrode array design or insertion technique.

In CI insertion experiments, ST phantoms are often used in place of cadaver cochleae. Synthetic phantoms have been developed or used by several research groups. Rebscher et al. [1] developed a transparent human ST phantom by making casts of human cadaver cochleae. The group created both epoxy and silicone elastomer phantoms, and a silicone phantom was used in insertion studies described in Refs. [2,3]. Included in Ref. [2] is a description of how the casts were measured to create a 3D digital model of the ST channel for use in evaluating electrode array designs. Zhang et al. created custom scaled-up prototype electrode arrays. They designed and used scaled 2D and 3D ST phantoms for insertion experiments using the custom arrays [4,5]. 2D phantoms from Cochlear™ (Sydney, NSW, Australia) were used in Refs. [6,7] for insertion studies. A 3D ST phantom from MED-EL (Innsbruck, Austria) was used in Refs. [8–11].

Each of the above phantoms can be useful for *in vitro* experimentation, but each has its limitations. 2D phantoms lack the true three-dimensional form of the human cochlea and do not offer a true representation of the ST's spiral form. The phantoms described in Ref. [1], cast from cadaver cochleae, offer accurate dimensions but are not reproducible without a physical mold. The group created a digital model of the ST channel, but we find no indication in the literature that this has been used or is available to create a phantom. The 3D phantom from MED-EL has a spiral shape, but from images of the phantom it appears that it does not faithfully represent ST dimensions along the channel length (e.g., the channel tapers too quickly) and it does not permit insertions past $1\frac{1}{4}$ turns. The method of ST modeling described in this paper is patterned after that employed by Zhang et al., but it is unclear from the literature whether their model took into account some shape and sizing aspects discussed herein. A 1:1 scale 3D phantom has been produced by Advanced Bionics (Valencia, CA) that allows insertion up to two turns into the channel, but creating a 1:1 scale CI prototype is sometimes difficult during the development of novel technology such as steerable CIs. We also do not know how accurate the model is or the exact method by which it was dimensioned and designed. The model described in this paper and the phantoms produced from the model address the limitations of current ST models and provide the following benefits:

- *Reproducibility*. The modeling method described in this paper can be reproduced using common engineering software and commonly available fabrication resources.
- *Accuracy*. The model represents a mean ST with size and shape informed by published anatomical data.
- *Scalability*. The model can be easily scaled to accommodate research needs.

2 Prior ST Models

Cohen et al. [12] described a method of fitting a template spiral to the shape of the images of implanted free-fitting CI electrode arrays. Radiographic images were selected from 30 CI patients, as well as images from nine cadaver temporal bones. For each radiograph, the positions of several points along each implanted array were digitized, and software was used to fit a mathematical spiral curve to the data for each array. The group found that the spiral shape of an implanted array could be modeled by the expressions

$$\theta < 100 \text{ deg}: \quad R = C(1 - D \ln(\theta - \theta_0)) \tag{1}$$

$$\theta \geq 100 \text{ deg}: \quad R = Ae^{-B\theta} \tag{2}$$

where R is the distance from the spiral center, θ is the angle in degrees, and A, B, C, D, and θ_0 are constants.

Yoo et al. [13] created a 3D model of the cochlea for viewing on the internet. Their model was based on the work done in Ref. [12], using Eqs. (1) and (2) and a height equation

$$z = E(\theta - \theta_1) \tag{3}$$

where z is the height value of each discrete spiral point, E is a constant, and θ_1 is the starting angular degree. The group used the resulting 3D spiral as the central path of their cochlea model with cross-section data from Ref. [14] to create a generalized 3D cochlea model (i.e., individual channels are not differentiated).

Zhang et al. [5] used the work of Refs. [12,13] to create 2D and 3D ST phantoms and used ST dimensions given by Wysocki [15] to define elliptical channel cross sections along the length of the 3D spiral curve. However, the authors did not publish the specifics of their model.

[1]Corresponding author.

Manuscript received September 21, 2010; final manuscript received October 23, 2010; published online January 6, 2011. Assoc. Editor: Gerald E. Miller.

Table 1 ST spiral constants

A (mm)	B (mm)	C (mm)	D (mm)	E (mm)	θ_0 (deg)	θ_1 (deg)	θ_f (deg)
3.762	0.001317	7.967	0.1287	0.003056	5.0	10.3	910.3

3 The ST Model

Using a method similar to the work of Zhang et al., we design a ST model based on Refs. [12,13,15] and include some modifications to increase the model's dimensional accuracy and qualitative appearance, as will be discussed hereafter.

Equations (1)–(3) are implemented in MATLAB to generate a 3D spiral path. The values for A, B, D, and θ_0 are given in Ref. [12], and the value for C is determined by setting Eqs. (1) and (2) equal to each other with $\theta=100$ deg and solving for C as described in Ref. [12]. The values for θ_1 and the final spiral angle, θ_f, are given in Ref. [13]. The value for the constant E is determined by solving Eq. (3) using the mean value of cochlear axial height, $z=2.75$ mm, and $\theta=\theta_f$ as described in Ref. [13]. The values for the constants listed above are given in Table 1. The constants given in Table 1 with Eqs. (1)–(3) can be used to create a 1:1 scale 3D spiral path. A scaling factor s can be used to scale the ST model (e.g., $s=3$ would create a 3:1 scale model). The values of R for discrete points along the curve are calculated using Eqs. (1)–(3), where θ varies from $\theta_1=10.3$ deg to $\theta_f=910.3$ deg in 0.1 deg increments. For each value of θ, the (x,y,z) coordinates of the corresponding 3D point on the curve are calculated using the equations

$$x = sR\cos(\theta) \tag{4}$$

$$y = sR\sin(\theta) \tag{5}$$

$$z = sE(\theta - \theta_1) \tag{6}$$

Several views of the 3D spiral path are shown in Fig. 1.

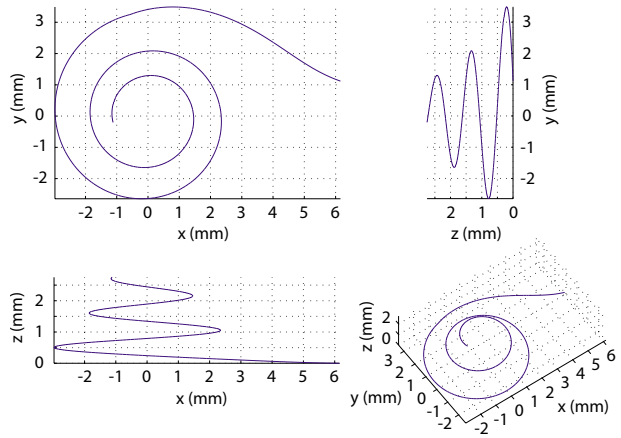

Fig. 1 1:1 scale 3D ST spiral path, generated in MATLAB

ST channel width and height dimensions for this model are based on the work by Wysocki et al. [15], who created latex casts of the human cochlea from 25 cadaver temporal bones and measured the width and height of the ST at 1 mm intervals along its length from the beginning of the ST. All but one of the values used in the model are channel dimensions given in plots in Ref. [15]. Due to construction difficulties in SolidWorks (Concord, MA) (i.e., failure when trying to create a lofted cut between the profiles) when using the given final channel width of about 1.45 mm, the value for the previous channel width (1.25 mm) is used as the final channel width. The channel dimensions are given in Table 2. ST dimensions given in Ref. [15] for 0 mm and 1 mm along the ST length are neglected in this model since the given ST height and width values for 0 mm are reported as zero, and there is a large jump in both width and height values between 0 mm and 2 mm along the ST length. Values in Table 2 from 0 mm to 34 mm along the spiral curve correspond to values from 2 mm to 36 mm measured along the ST length given in Ref. [15]. Note that the values do not change monotonically. The height, width, and posi-

Table 2 ST channel dimensions, based on Ref. [15]. Position (Pos) is measured along the spiral from the basal end ($\theta=10.3$ deg), h=profile height, w=profile width, and ϕ=profile tilt angle relative to the xy-plane.

Pos (mm)	0	1	2	3	4	5	6	7	8	9	10	11	12	13	14
h (mm)	1.30	1.18	1.14	1.13	1.08	1.03	0.98	0.94	0.90	0.86	0.84	0.83	0.82	0.82	0.81
w (mm)	2.10	2.10	1.95	1.85	1.80	1.74	1.70	1.68	1.63	1.60	1.59	1.51	1.50	1.54	1.46
ϕ (rad)	0	0.01	0.02	0.03	0.04	0.05	0.06	0.07	0.08	0.09	0.10	0.11	0.12	0.13	0.14
Pos (mm)	15	16	17	18	19	20	21	22	23	24	25	26	27	28	29
h (mm)	0.81	0.79	0.77	0.75	0.73	0.72	0.67	0.66	0.63	0.59	0.54	0.47	0.43	0.37	0.34
w (mm)	1.45	1.43	1.38	1.33	1.32	1.31	1.30	1.30	1.30	1.30	1.30	1.30	1.30	1.31	1.31
ϕ (rad)	0.15	0.16	0.17	0.18	0.19	0.20	0.21	0.22	0.23	0.24	0.25	0.26	0.27	0.28	0.29
Pos (mm)	30	31	32	33	34										
h (mm)	0.29	0.28	0.26	0.35	0.30										
w (mm)	1.26	1.15	1.23	1.25	1.25										
ϕ (rad)	0.30	0.25	0.20	0.15	0.10										

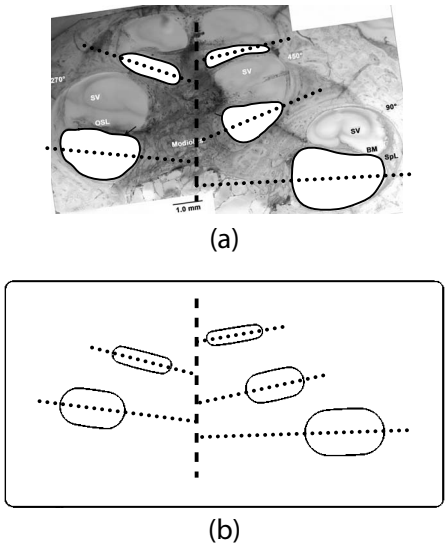

Fig. 2 Cross sections showing ST channel profile outlines and tilt angles (dotted lines). The dashed vertical lines represent the cochlear central spiral axis. (*a*) Photograph of cochlea cross section (public domain image from Ref. [3]), with ST profiles outlined. (*b*) Model cross section.

tion values are multiplied by the scaling factor s so that scaling is correctly applied to dimension the ST channel profiles to place them at regular intervals along the spiral curve.

Zhang et al. [5] modeled the ST channel cross sections as ellipses. However, we model the ST cross sections as semicircular ends connected by straight segments, which we believe more closely match the general ST channel cross-section outline, as shown in Fig. 2. A profile tilt angle ϕ between the xy-plane and the major axis of the cross section is set for each profile to qualitatively approximate the angle observed in many cochlea cross-sectional views, in which the profile cross-section width directions are not perpendicular to the cochlea central spiral axis, as shown in Fig. 2. A profile example is shown in Fig. 3, with the angle ϕ

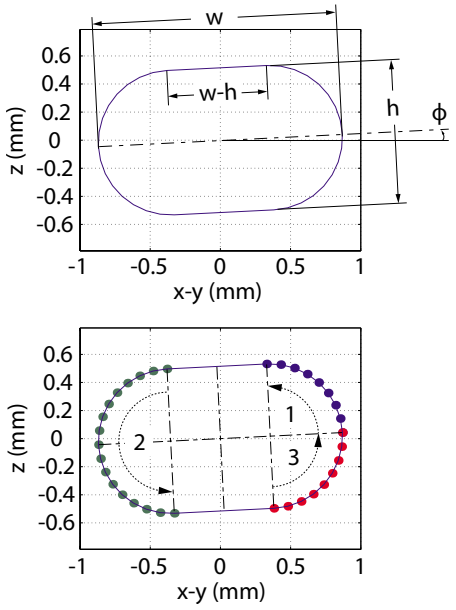

Fig. 3 ST channel profile example. (top) Profile showing width (*w*), height (*h*), and angle (ϕ) of the profile relative to the xy-plane. (bottom) Order in which profile points are plotted: 1 (Eq. (8)), 2 (Eq. (9)), and 3 (Eq. (10)).

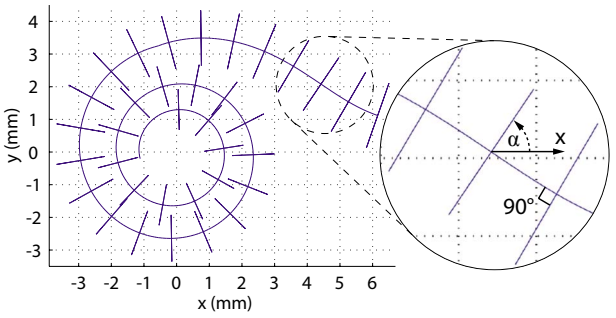

Fig. 4 ST spiral curve with profiles positioned along its length. The channel profile angle α is shown, defined relative to the positive x-axis direction.

defined relative to the xy-plane. The ϕ values used in this model are included in Table 2.

Our first goal is to place the cross sections along the length of the spiral curve, while temporarily neglecting their radial positioning. Ultimately, we are only concerned with the final placement of the cross sections and not with the spiral path itself. The discrete point along the curve which is used as the coordinate center of each cross-section profile is found based on the summed length of the path segments from the beginning of the curve to each point. The angle α of each profile relative to the model coordinate frame x-axis is also determined (Fig. 4). This is done by finding the direction of the xy-plane projection of the spiral curve that passes through each profile and rotating the direction by $\pi/2$ rad clockwise using the equation

$$\alpha = \text{atan2}(\Delta y, \Delta x) - \pi/2 \tag{7}$$

where α is the angle of the profile projection onto the xy-plane with respect to the x-axis, atan2 is the four-quadrant inverse tangent function, and Δy and Δx are the differences between the y and x coordinates of the center of the profile and the successive discrete point on the spiral curve. This effectively places each profile perpendicular to the xy-plane projection of the spiral curve passing through it.

To create the oblong channel profiles, points defining each profile, with profile center (0,0), are calculated using the following equations inspired by ellipse equations: For $0 \le \theta \le \pi/2$,

$$x = \frac{w-h}{2}\cos(\phi) + \frac{h}{2}\cos(\theta+\phi)$$

$$z = \frac{w-h}{2}\sin(\phi) + \frac{h}{2}\sin(\theta+\phi) \tag{8}$$

For $\pi/2 \le \theta \le 3\pi/2$,

$$x = \frac{w-h}{2}\cos(\pi+\phi) + \frac{h}{2}\cos(\theta+\phi)$$

$$z = \frac{w-h}{2}\sin(\pi+\phi) + \frac{h}{2}\sin(\theta+\phi) \tag{9}$$

For $3\pi/2 \le \theta \le 2\pi$,

$$x = \frac{w-h}{2}\cos(\phi) + \frac{h}{2}\cos(\theta+\phi)$$

$$z = \frac{w-h}{2}\sin(\phi) + \frac{h}{2}\sin(\theta+\phi) \tag{10}$$

where w and h are the width and the height of a given profile, θ varies from 0 rad to 2π rad in increments of $\pi/16$ rad in the sets shown in Fig. 3, and ϕ is the tilt angle (rad) of a given profile. Note that two points are calculated at three angles: $\theta = 0, 2\pi$, θ

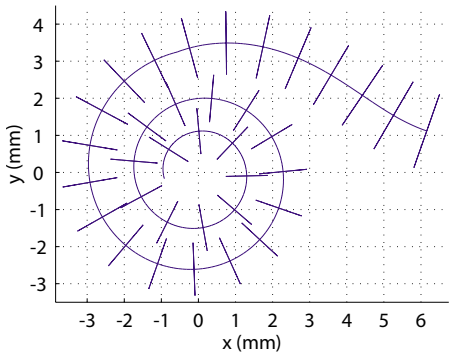

Fig. 5 ST spiral curve with profiles centered, after spiral tightening to position the final profile closer to the curve apex

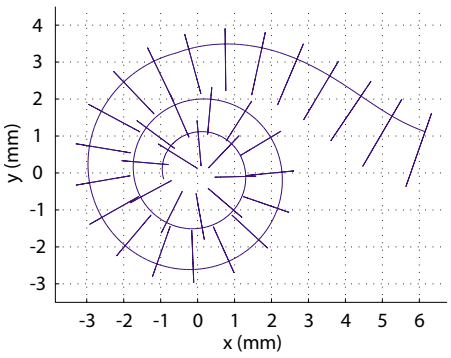

Fig. 6 ST spiral curve with profiles shifted to decrease the length of the ST inner and outer walls. Compare with original model of Fig. 4 and intermediate model of Fig. 5.

$=\pi/2$, and $\theta=3\pi/2$. A solid profile outline is formed (Fig. 3) when the profile points are plotted in the order shown. Next, the individual 2D profiles of Fig. 3 are converted to the true 3D profiles, as shown in Fig. 4. Arrays containing the (x_{pc}, y_{pc}, z_{pc}) coordinates, defining each profile in its correct 3D position and orientation, are then formed using the equations

$$x_{pc} = X_c + x\cos(\alpha) \tag{11}$$

$$y_{pc} = Y_c + x\sin(\alpha) \tag{12}$$

$$z_{pc} = Z_c + z \tag{13}$$

where x_{pc}, y_{pc}, and z_{pc} contain the coordinates of each calculated profile point with the profile positioned so that the ST spiral curve passes through its center; X_c, Y_c, and Z_c are the coordinates of the center of the profile; x and z contain the profile points calculated using Eqs. (8)–(10); and α is the orientation angle of the profile (see Eq. (7) and Fig. 4).

Figure 4 shows the ST cross-section profiles placed along the spiral curve, with the curve passing through the profile centers. It can be seen in the figure that the final profile is not as close to the apex of the spiral path as it should be. We want to keep the profiles spaced at 1 mm increments along the curve as we shift them closer to the curve apex, which can be achieved by tightening the spiral. Recall that the spiral path from Ref. [12] was not intended to be used to describe the center of the ST channel, so some necessary tightening is expected. To tighten the spiral, the implementation of Eq. (2) is modified to incrementally enhance the decrease in R as θ increases by changing the value used for θ. The modification can be modeled by the empirical expression

$$\theta_{\text{mod}} = 0.0002\theta^2 + 0.98\theta \tag{14}$$

The calculation of R in Eqs. (1) and (2) should use this θ_{mod}. The tightened curve with positioned cross-section profiles is shown in Fig. 5.

With the profiles centered along the spiral path, the inner and outer walls of the channel formed by the ST cross sections measure 24.92 mm and 43.13 mm, respectively. These values exceed those of Ref. [16], which reports inner and outer ST wall lengths of $18.29\ \text{mm} \pm 1.47\ \text{mm}$ and $40.81\ \text{mm} \pm 1.97\ \text{mm}$, respectively. This is again a logical and expected result, since Eqs. (1) and (2) give a mean template spiral for electrode arrays positioned close to the ST outer-wall, not along the ST center. Accordingly, we shift the cross-section profiles inward, positioning the template spiral closer to the ST outer wall, and decreasing the ST inner- and outer-wall lengths. Each profile is shifted by a fraction of its width along the directions corresponding to the dotted lines in Fig. 2(*b*). Shifting the profiles by 1/4 of their respective widths achieves the desired result. The shifted coordinates for each profile are calculated using the equations

$$x_{ps} = x_{pc} - \frac{w}{4}\cos(\alpha)\cos(\phi) \tag{15}$$

$$y_{ps} = y_{pc} - \frac{w}{4}\sin(\alpha)\cos(\phi) \tag{16}$$

$$z_{ps} = z_{pc} - \frac{w}{4}\sin(\phi) \tag{17}$$

where x_{ps}, y_{ps}, and z_{ps} contain the shifted coordinates of each calculated point defining the profile; x_{pc}, y_{pc}, and z_{pc} are as previously defined; w is the profile width; and ϕ and α are the profile tilt and orientation angles as previously defined. Shifting the profiles yields a model with a ST inner-wall length of 20.55 mm and a ST outer-wall length of 38.54 mm, which are close to the values given in Ref. [16]. A view of the shifted profiles positioned along the length of the spiral curve is shown in Fig. 6.

4 Fabrication of a ST Phantom

A 3:1 scale 3D solid model was created in SolidWorks. The points generated for each ST profile were imported into SolidWorks as curves through XYZ points. A rectangular prism was created around the imported profiles, with the most basal profile positioned slightly outside of the prism. The ST channel was formed by creating a lofted cut connecting the profiles. Figure 7 shows the imported profiles and channel formed by the lofted cut. The apical end of the channel was rounded by creating a sketch of half of the most apical channel profile and creating a 180 deg revolved cut, resulting in a semicircular end, as shown in Fig. 8.

A 1 mm diameter access hole was created from the face of the model extending into the semicircular end of the channel. This hole facilitates injection of soap solution into the channel, which

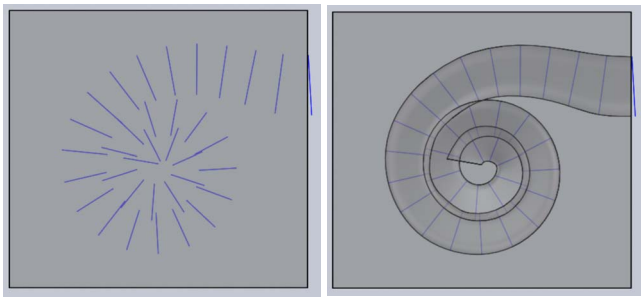

Fig. 7 Views of SolidWorks model construction. (left) Imported channel profiles with surrounding rectangular prism. (right) Channel formed by connecting the profiles with a lofted cut.

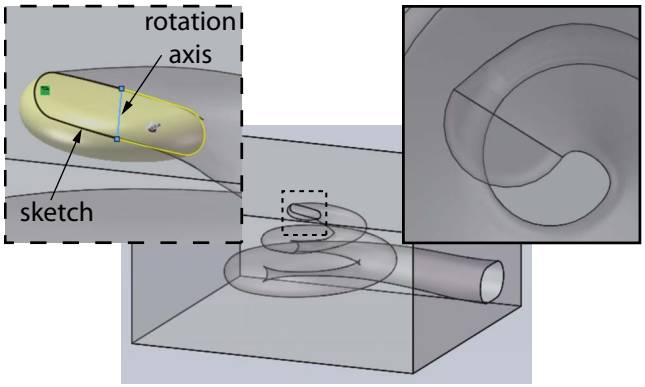

Fig. 8 Semicircular cut created at the ST channel apical end. (inset, dashed border) Sketch and rotation axis used to create the revolved cut. (inset, solid border) Semicircular end.

is a standard method to lubricate phantoms for *in vitro* insertions. The hole can be plugged after injecting the soap solution to avoid leaking. A mounting tab was created so that the phantom could be mounted for experiments. Using the generated 3D model, a phantom was manufactured by Javelin 3D (Park City, UT) using an Objet 3D printer. Images of the phantom are shown in Fig. 9. The 1 mm access hole and mounting tab can be seen in several views.

5 Conclusions

A scala-tympani phantom can be fabricated using the model created here, which was synthesized from published anatomical data. The model can be scaled to meet research needs. MATLAB code and a SolidWorks model file can be downloaded from the University of Utah Telerobotics Laboratory web page [17].

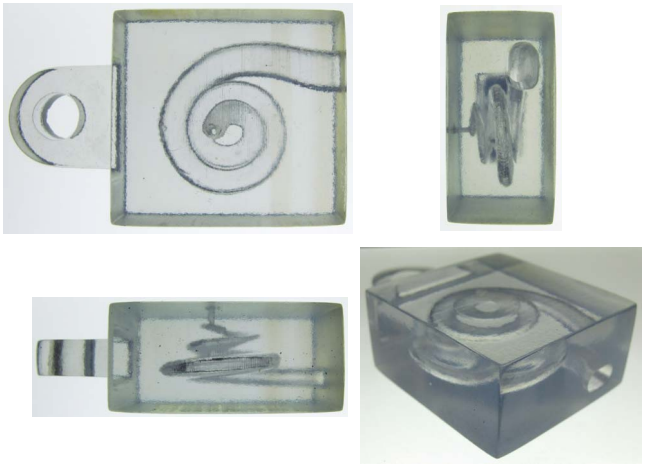

Fig. 9 Fabricated 3:1 scale ST phantom. The rectangular prism has dimensions $31 \times 29 \times 15$ mm^3.

Acknowledgment

This work was supported in part by the National Science Foundation under Grant No. IIS-0952718. This research is part of a larger collaboration with Dr. Robert Webster at Vanderbilt University, and the authors would like to thank him for fruitful discussions.

References

[1] Rebscher, S. J., Talbot, N., Bruszewski, W., Heilmann, M., Brasell, J., and Merzenich, M. M., 1996, "A Transparent Model of the Human Scala Tympani Cavity," J. Neurosci. Methods, **64**, pp. 105–114.
[2] Rebscher, S. J., Heilmann, M., Bruszewski, W., Talbot, N. H., Snyder, R. L., and Merzenich, M. M., 1999, "Strategies to Improve Electrode Positioning and Safety in Cochlear Implants," IEEE Trans. Biomed. Eng., **46**(3), pp. 340–352.
[3] Rebscher, S. J., Hetherington, A., Bonham, B., Wardrop, P., Whinney, D., and Leake, P. A., 2008, "Considerations for Design of Future Cochlear Implant Electrode Arrays: Electrode Array Stiffness, Size, and Depth of Insertion," J. Rehabil. Res. Dev., **45**, pp. 731–748.
[4] Zhang, J., Roland, J. T., Jr., Simaan, N., and Manolidis, S., 2006, "A Pilot Study of Robot-Assisted Cochlear Implant Surgery Using Steerable Electrode Arrays," MICCAI 2006, Paper No. LNCS 4190, pp. 33–40.
[5] Zhang, J., Roland, J. T., Jr., Manolidis, S., and Simaan, N., 2009, "Optimal Path Planning for Robotic Insertion of Steerable Electrode Arrays in Cochlear Implant Surgery," ASME J. Med. Devices, **3**, p. 011001.
[6] Zhang, J., Bhattacharyya, S., and Simaan, N., 2009, "Model and Parameter Identification of Friction During Robotic Insertion of Cochlear-Implant Electrode Arrays," IEEE International Conference on Robotics and Automation, pp. 3528–3533.
[7] Todd, C. A., Naghdy, F., and Svehla, M. J., 2007, "Force Application During Cochlear Implant Insertion: An Analysis for Improvement of Surgeon Technique," IEEE Trans. Biomed. Eng., **54**(7), pp. 1247–1255.
[8] Mirzadeh, H., and Abbasi, F., 2004, "Segmented Detachable Structure of Cochlear-Implant Electrodes for Close-Hugging Engagement With the Modiolus," J. Biomed. Mater. Res., Part B: Appl. Biomater., **68B**(2), pp. 191–198.
[9] Hussong, A., Rau, T., Eilers, H., Baron, S., Heimann, B., Leinung, M., Lenarz, T., and Majdani, O., 2008, "Conception and Design of an Automated Insertion Tool for Cochlear Implants," IEEE/EMBS Annual International Conference, pp. 5593–5596.
[10] Majdani, O., Schurzig, D., Hussong, A., Rau, T., Wittkopf, J., Lenarz, T., and Labadie, R. F., 2010, "Force Measurement of Insertion of Cochlear Implant Electrode Arrays In Vitro: Comparison of Surgeon to Automated Insertion Tool," Acta Oto-Laryngol., **130**, pp. 31–36.
[11] Schurzig, D., Labadie, R. F., Hussong, A., Rau, T. S., and Webster, R. J., III, 2010, "Design of a Tool Integrating Force Sensing With Automated Insertion in Cochlear Implantation," IEEE/ASME Trans. Mechatron., in press.
[12] Cohen, L. T., Xiu, J., Xu, S. A., and Clark, G. M., 1996, "Improved and Simplified Methods for Specifying Positions of the Electrode Bands of a Cochlear Implant Array," Am. J. Otol., **17**, pp. 859–865.
[13] Yoo, S. K., Wang, G., Rubinstein, J. T., Skinner, M. W., and Vannier, M. W., 2000, "Three-Dimensional Modeling and Visualization of the Cochlea on the Internet," IEEE Trans. Inf. Technol. Biomed., **4**(2), pp. 144–151.
[14] Gulya, A. J., and Steenerson, R. L., 1996, "The Scala Vestibuli for Cochlear Implantation: An Anatomic Study," Arch. Otolaryngol. Head Neck Surg., **122**, pp. 130–132.
[15] Wysocki, J., 1999, "Dimensions of the Human Vestibular and Tympanic Scalae," Hear. Res., **135**, pp. 39–46.
[16] Kawano, A., Sheldon, H. L., and Clark, G. M., 1996, "Computer-Aided Three-Dimensional Reconstruction in Human Cochlear Maps: Measurement of the Lengths of Organ of Corti, Outer Wall, Inner Wall, and Rosenthal's Canal," Ann. Otol. Rhinol. Laryngol., **105**, pp. 701–709.
[17] University of Utah Telerobotics Laboratory, http://www.telerobotics.utah.edu/